# Delft University of Technology

# Why do published models for fluvial and estuarine morphodynamics use unrealistic representations of the effects of transverse bed slopes?

Tritthart, Michael; Vanzo, Davide; Chavarrías, Victor; Siviglia, Annunziato; Sloff, Kees; Mosselman, Erik

**Important note**
To cite this publication, please use the final published version (if applicable).
Please check the document version above.

# Why do published models for fluvial and estuarine morphodynamics use unrealistic representations of the effects of transverse bed slopes?

Michael Tritthart [a],[*], Davide Vanzo [b],[c], Victor Chavarrías [d], Annunziato Siviglia [f], Kees Sloff [d],[e], Erik Mosselman [d],[e]

[a] University of Natural Resources and Life Sciences, Vienna, Department of Water, Atmosphere and Environment, Institute of Hydraulic Engineering and River Research, Am Brigittenauer Sporn 3, 1200 Vienna, Austria
[b] ETH - Swiss Federal Institute of Technology, Laboratory of Hydraulics, Hydrology and Glaciology, Hönggerbergring 26, 8093, Zürich, Switzerland
[c] Karlsruhe Institute of Technology, Institute for Water and Environment, Kaiserstrasse 12, 76131 Karlsruhe, Germany
[d] Deltares, Department of River Dynamics and Inland Shipping, Boussinesqweg 1, 2629 HV Delft, The Netherlands
[e] Delft University of Technology, Department of Hydraulic Engineering, Stevinweg 1, 2628 CN Delft, The Netherlands
[f] University of Trento, Department of Civil, Environmental and Mechanical Engineering, Via Mesiano 77, 38123 Trento, Italy

## ARTICLE INFO

## ABSTRACT

The sediment transport direction is affected by the bed slope. This effect is of crucial importance for two- and three-dimensional modelling of the interaction between the flow of water and the alluvial bed. It is not uncommon to find applications of numerical morphodynamic models in the literature that exaggerate the effects of transverse bed slopes on sediment transport compared to results from laboratory experiments. We investigate mathematically the consequences of such an approach, and we analyse through numerical simulations different explanations for the need to apply deviating values. The study reveals that the reason often lies in the setup of the numerical models, such as the choice of mesh resolution or the necessity to comply with specific aspects of the numerical scheme. The missing or inadequate implementation of physical processes in the model is another cause. All of these effects can be compensated by artificial diffusion added through the bed slope effect coefficients. Since increased diffusion strongly alters the physical processes of self-formed bed morphology, we recommend that modellers address the root causes of inflated erosion and deposition. Bed slope effect coefficients should be applied within the range found in the original publications.

## 1. Introduction

With the advance of numerical models for sediment transport and morphodynamics into engineering practice, questions about accuracy and correct use of such models need to be addressed. These models usually simulate some or all of the following processes: (i) bedload transport, (ii) suspended load transport, (iii) morphodynamics and (iv) sorting processes of sediment at the river bed (e.g. Siviglia and Crosato, 2016; Williams et al., 2016). Morphodynamic simulations are typically based on the sediment mass balance equation (Exner, 1920 equation), and require the underlying transport processes to be correctly modelled.

Since most of the transport equations for bedload (e.g. Meyer-Peter and Müller, 1948; Engelund and Hansen, 1967; van Rijn, 1993) were originally derived for a flat bed, the transport capacities delivered by the models need to be corrected for slope, both in longitudinal and lateral direction. There is long-standing evidence in literature that morphodynamic simulations of the evolution of the bed of rivers and

estuaries depend sensitively on parameters of the submodel for the effect of transverse bed slopes on the direction of sediment transport (e.g. Marciano et al., 2005; Schuurman et al., 2013; Baar et al., 2019). Even more, two- and three-dimensional morphodynamic models must consider the effect of the bed slope in the sediment transport to be well-posed (Chavarrías et al., 2019). This bed slope effect is the main damping mechanism in the formation of patterns of bars and channels (e.g. Blondeaux and Seminara, 1985; Colombini et al., 1987). Sediment particles pulled down by gravity reduce bar heights and fill the channels. Only the consideration of the bed slope effect allows the correct prediction of sediment particle paths in rivers (Tritthart et al., 2019a) and ensuing morphodynamics.

Literature suggests that achieving realistic results in morphodynamic simulations for rivers and estuaries sometimes requires assigning bed slope effect parameters values that significantly differ from those obtained through experimental methods (e.g. Nicholas et al., 2013; van der Wegen and Jaffe, 2014; van Dijk et al., 2019). In particular,

---

to achieve morphodynamic results which align more with observations or expected outcomes of bed evolution, researchers and practitioners deliberately increase the proportion of sediment which is transported laterally.

The effect of the transverse bed slope on the direction of the sediment transport has been modelled in similar ways by different authors (van Bendegom, 1947; Koch and Flokstra, 1981; Ikeda, 1982). Beyond the specific formulation, the magnitude of the lateral deviation scales with a calibration factor, with value ranges provided in the derivation of the different models. For the sake of clarity, we refer to this non-dimensional factor as the *transverse bed slope factor* $F_{TBS}$ throughout the paper.

Baar et al. (2019) argue that higher $F_{TBS}$ values are needed to counter a tendency to incise due to an apparent preference of the water to flow through as few grid cells as possible. They also explain that higher $F_{TBS}$ values are needed if the bed slope effect is applied to the bedload part of the sediment transport alone, and find empirically that the required increase of $F_{TBS}$ is related to grid size. They conclude that it is impossible to have realistic sediment transport vectors and morphology in the same model study. However, there are also other potential explanations, ranging from poor representation of physical processes to problems with the numerical implementation. Regarding the first point, an example in morphodynamic modelling can be found in the misuse of the spatial and temporal adaptation of sediment transport to capacity conditions for improving the results (Mosselman and Le, 2015). Inertia of the sediment particles cause a lag between bed shear stress and sediment transport, which can be modelled by means of a relaxation equation (Bell and Sutherland, 1983; Phillips and Sutherland, 1989; Jain, 1992). In field applications, sediment transport can usually be assumed to adapt instantly to capacity conditions given that the sediment transport adaptation length is short compared to usual grid sizes and the adaptation time is short compared to the time step. An unrealistically large sediment transport adaptation length has the effect of dampening perturbations and smoothing results, which may be desired for counteracting the effects of an unstable numerical scheme. Regarding the second point, numerical models are approximate solutions that suffer from *numerical diffusion*, which depends on the numerical scheme and the grid resolution. Numerical diffusion works in the same direction as lateral transport, thus it can induce non-physical lateral transport rates, which however may assist in reaching a smoother bed morphology when it is artificially increased.

In this paper we systematically analyse different explanations for the need to apply deviating values of $F_{TBS}$. We argue that exaggerating the bed slope effect is needed to correct inadequate representation of other mechanisms and physical processes in the models. The aim of this paper is to provide a synthetic analysis of the physical meaning and numerical modelling consequences when using a transverse bed slope factor. Moreover, it invites the reader to a careful interpretation of its usage, and provides examples of unforeseen consequences when tweaking its value.

The paper is structured as follows: we first briefly recall the physical meaning of the transverse bed slope factor and its critical relevance in determining self-formed morphology (Section 2). Section 3 shows how the sediment transport deviation, hence the transverse bed slope factor, is inherently connected to multiple aspects of the adopted numerical solutions. We use four different numerical solvers to show that no particular software is favoured and that the findings here presented are to be considered general. The conclusions of this manuscript do not depend on the application of any specific software system. The interested reader can refer to the Appendix for details of the software used. Lastly, we disentangle and discuss how the transverse bed slope factor might be used (and mis-used) to compensate the missing implementation of different physical processes, and how this can lead to unforeseen and non-realistic morphodynamic solutions (Sections 4 and 5).
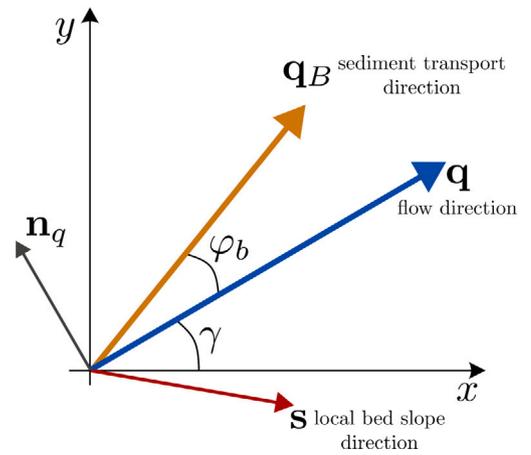


**Fig. 1.** Directions of sediment transport applying the transverse bed slope effect.

## 2. Theoretical background

Numerical models to simulate the evolution of alluvial riverbeds are based on an equation for the conservation of sediment mass. Although historically not correct (cf. Barneveld et al., 2023, 2024), we here refer to this as the Exner equation. In the horizontal $x$, $y$ plane it can be expressed as:

$$(1 - p)\frac{\partial z_b}{\partial t} + \frac{\partial q_{B_x}}{\partial x} + \frac{\partial q_{B_y}}{\partial y} = S_b, \tag{1}$$

where $z_b(x, y, t)$ is the bed elevation, the unknown of the problem, $p$ [-] is the bed porosity, assumed here constant in space and time, $S_b$ [m/s] is an external source term specifying inputs or outputs of sediment material (e.g. slope collapse, excavation or interaction with sediment in suspension), and $\mathbf{q}_B = (q_{B_x}, q_{B_y})$ [m²/s] is the specific sediment transport rate. For the sake of simplicity, we neglect the external source and assume the porosity included in the sediment transport predictor. The magnitude of the transport rate vector $\mathbf{q}_B$ is evaluated via experimental closure relationships available in literature (e.g. Meyer-Peter and Müller, 1948; Engelund and Hansen, 1967; Ashida and Michiue, 1971; Wilcock and Crowe, 2003). The direction of the sediment transport is assumed to locally align with the direction of the flow (direction of vector $\mathbf{q}$ in Fig. 1), providing the drag force. The presence of a lateral (i.e., transverse) bed slope with respect to the flow direction causes a deviation of the sediment flux by an angle $\varphi_b$, as depicted in Fig. 1. Such deviation angle can be expressed as

$$\tan \varphi_b = \frac{1}{f} \cdot \mathbf{s} \cdot \mathbf{n}_q, \text{ for } \mathbf{s} \cdot \mathbf{n}_q < 0, \tag{2}$$

where $f$ [$-$] is a function derived experimentally, $\mathbf{s} = \left(\frac{\partial z_b}{\partial x}, \frac{\partial z_b}{\partial y}\right)$ is the local bed slope and $\mathbf{n}_q = (-\sin \gamma, \cos \gamma)$ is the unit vector perpendicular to $\mathbf{q}$ in downhill direction; $\gamma$ represents the direction of liquid discharge $\mathbf{q}$ (see Fig. 1).

Two fundamentally different methods are available to consider the transverse bed slope effect: (a) direction-based; (b) magnitude-based. Direction-based approaches rotate the transport vector according to the local bed slope and do not modify the transport vector's magnitude. This concept originates from van Bendegom (1947), who defined

$$\tan \varphi_b = -\frac{1}{f(\theta)} \frac{\partial z_b}{\partial n}, \tag{3}$$

thereby postulating a dependence of $f$ on the Shields (1936) parameter $\theta$ [$-$]; $n$ denotes the transverse coordinate. Koch and Flokstra (1981) determined the relation $f = 1.7\theta^{0.5}$. Struiksma and Crosato (1989) analysed data from a circular flume experiment performed by Zimmerman and Kennedy (1978) and obtained $f = 0.85\theta^{0.5}$. Talmon et al. (1995) explained the lower coefficient from bed form heights in laboratory

flumes being exaggerated compared to natural rivers, resulting in a smaller $f$ and thus larger bed slope effect. They also performed experiments using different grain size fractions ranging from fine sand to coarse sand and suggested the relation $f = 9 \left( \frac{d_{50}}{h} \right)^{0.3} \theta^{0.5}$, using the median particle diameter $d_{50}$ and the water depth $h$ to introduce a relative particle size into the equation. However, because of the simplicity of the equation, the relation

$$f = A\theta^B \tag{4}$$

is used more often, with $B = 0.5$ and $A = 0.85$ (default values in the Delft3D code, as an example) . It should be noted that for natural rivers this default value already corresponds to an exaggeration of the transverse bed slope effect by a factor of 2 compared to the original relation determined by Koch and Flokstra (1981).

In contrast to the direction-based transport approach, Ikeda (1982) proposed a magnitude-based approach. In this type of consideration of the transverse bed slope effect, an additional bedload transport vector is calculated perpendicular to the direction of the (original) bedload transport vector. Its magnitude $\alpha_n$ is derived from

$$\alpha_n = \varepsilon \left( \frac{\tau_{b,cr}}{\tau_b} \right)^{0.5} \frac{\partial z_b}{\partial n}, \tag{5}$$

where $\tau_b$ and $\tau_{b,cr}$ are the bed shear stress and critical bed shear stress, respectively, and $\varepsilon$ is a user-specified tuning parameter, with a default value of $\varepsilon = 1.5$. The bed shear stress and critical bed shear stress can be replaced by the corresponding Shields parameter $\theta$ and critical Shields parameter $\theta_{cr}$, respectively. With $\alpha_n = -\tan\varphi_b$, Eq. (2) can be rewritten as

$$f = \frac{1}{\varepsilon} \left( \frac{\theta}{\theta_{cr}} \right)^{0.5}. \tag{6}$$

In addition to the rotation, however, the magnitude of the bedload transport vector is increased in this approach. An increase of $\varepsilon$ results in an increase of the effect of lateral bed slopes. With an approximate value of $\theta_{cr} = 0.05$ for gravel and the suggested default value $\varepsilon = 1.5$, we obtain $A \approx 3.0$ in Eq. (4).

To summarize, the transverse bed slope effect is proportional to a function $1/f$ of the flow and sediment characteristics tuned with an experimental non-dimensional factor (e.g. $\varepsilon$ or $1/A$). To evaluate the effect of increasing or scaling the transverse bed slope factor, we simply introduce in our notation the multiplicator $F_{\text{TBS}}$, such that the lateral transport function reads $F_{\text{TBS}}/f$, with $F_{\text{TBS}} = 1$ corresponding to the original formulation of the authors. By substitution in (2), the approach reads:

$$\tan\varphi_b = \frac{F_{\text{TBS}}}{f} \left( -\frac{\partial z_b}{\partial x} \sin\gamma + \frac{\partial z_b}{\partial y} \cos\gamma \right). \tag{7}$$

If we cast the direction according to the transverse bed slope effect (Fig. 1) in the original Exner Eq. (1), we obtain:

$$\frac{\partial z_b}{\partial t} + \frac{\partial}{\partial x} \left[ \frac{q_B}{q} \left( q_x \cos\varphi_b - q_y \sin\varphi_b \right) \right] + \frac{\partial}{\partial y} \left[ \frac{q_B}{q} \left( q_x \sin\varphi_b + q_y \cos\varphi_b \right) \right] = 0, \tag{8}$$

where $q_B$ and $q$ are the magnitudes of the sediment and flow flux vectors. From literature, Eq. (2) is assumed valid for small deviation angles $\varphi_b$; it follows that we can assume $\tan\varphi_b \approx \sin\varphi_b$ and $\cos\varphi_b \approx 1$. In this way, it is easy to substitute (7) into (8), and to obtain a reduced version of the Exner equation, valid for small deviation angles:

$$\frac{\partial z_b}{\partial t} + \frac{\partial}{\partial x} \left[ \frac{q_B}{q} q_x + \frac{F_{\text{TBS}}}{f} \left( \frac{q_B q_y^2}{q^2} \frac{\partial z_b}{\partial x} - \frac{q_B q_x q_y}{q^2} \frac{\partial z_b}{\partial y} \right) \right] + \frac{\partial}{\partial y} \left[ \frac{q_B}{q} q_y + \frac{F_{\text{TBS}}}{f} \left( \frac{q_B q_x^2}{q^2} \frac{\partial z_b}{\partial y} - \frac{q_B q_x q_y}{q^2} \frac{\partial z_b}{\partial x} \right) \right] = 0. \tag{9}$$

For the sake of simplification, let us consider a case where the flow is in $x$ direction, hence $q = q_x$, $q_y = 0$. Eq. (9) simplifies further in:

$$\frac{\partial z_b}{\partial t} + \frac{\partial q_B}{\partial x} + \frac{\partial}{\partial y} \left[ \frac{F_{\text{TBS}}}{f} \left( q_B \frac{\partial z_b}{\partial y} \right) \right] = 0. \tag{10}$$

The third term contains the second derivative of the bed elevation with respect to $y$, so the lateral slope effect represents a diffusive term in the Exner equation. It is worth pointing out: (i) the slope effect is not influencing the "advection" of the sediment flux in the dominant flow direction ($x$ in this case), (ii) a deliberately high value of $F_{\text{TBS}}$ can lead to an unphysical situation where the diffusive term in the lateral direction ($y$) is larger than the advective term, (iii) if the diffusive term is dominant (increasing with $F_{\text{TBS}}$), a numerical solver for hyperbolic equations would not be the correct tool, and might result in non-converging or unstable numerical solutions. The above-mentioned behaviour can be further recast in terms of the Péclet number. Let us linearize Eq. (10) as follows:

$$\frac{\partial z_b'}{\partial t} + \lambda \frac{\partial z_b'}{\partial x} + D \frac{\partial^2 z_b'}{\partial y^2} = 0, \tag{11}$$

where $\lambda = \partial q_B / \partial z_b$ represents the advection velocity and $D = F_{\text{TBS}} \cdot q_B / f$ the diffusion rate of the model Eq. (11), and $'$ has been used to identify a perturbed variable. In this linearized form, the Péclet number reads:

$$\text{Pe} = \frac{W\lambda}{D} = \frac{1}{F_{\text{TBS}}} \frac{W\lambda f}{q_B}, \tag{12}$$

having $W$ [m] as representative length scale for sediment transport (e.g., channel width). From (12), it is evident how an artificial increment of $F_{\text{TBS}}$ results in a hyperbolic decay of the Péclet number. Without changing any physical parameter (e.g., $q_B$), by artificially altering the transverse bed slope factor, the governing sediment transport Eq. (11) can turn from advection-dominated (Pe $\rightarrow$ inf) to a diffusion-dominated problem (Pe $\rightarrow 0$).

## 3. Numerical aspects

The choice of $F_{\text{TBS}}$ directly affects the mathematical character of the problem at hand. The diffusion aspect of the Exner equation, which results from incorporating a transverse bed slope effect, has varying implications for the numerical solution of the Exner problem. These implications depend on the type and resolution of the computational meshes and the chosen numerical scheme for integrating the Exner equation.

### 3.1. Mesh resolution

A first challenge is related to the varying relative intensity between physical diffusion due to the lateral transport (which scales with $F_{\text{TBS}}$) and the numerical diffusion (see Bailey, 2017; Vanzo et al., 2017). Numerical approximation of partial differential equations (PDE), as for the Exner equation, results invariably in numerical diffusion (or dissipation, e.g. Toro, 2009). The magnitude of numerical diffusion depends on the numerical integration strategy and it is not possible to derive a general formulation. Nevertheless, it increases for increasing grid size, holding other factors constant.

#### 3.1.1. One-dimensional considerations

For the case of a first-order upwind and forward in time explicit scheme for the one-dimensional linear Exner equation, the numerical diffusion can be analytically derived. The linear Exner equation reads (see Eq. (11)):

$$\frac{\partial z_b'}{\partial t} + \lambda \frac{\partial z_b'}{\partial x} = 0, \tag{13}$$

We consider a wave-like solution:

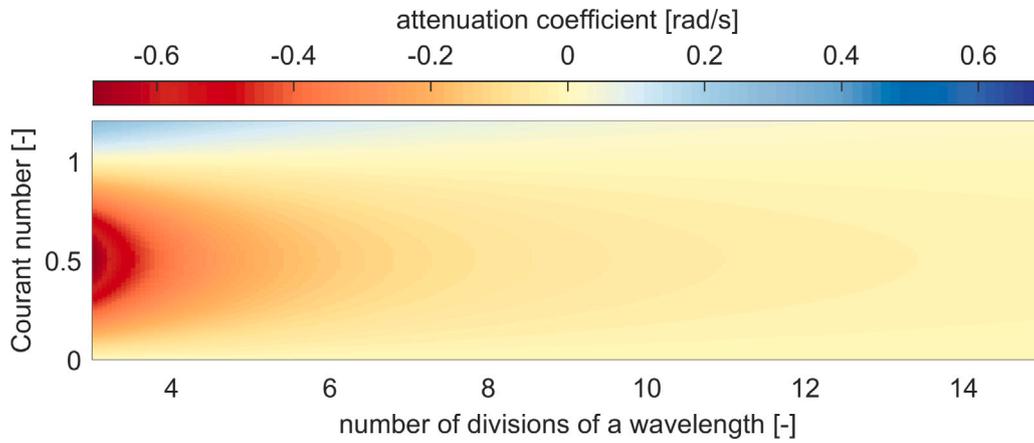$$z_b' = A e^{i(kx - \omega t)}, \tag{14}$$

**Fig. 2.** Attenuation coefficient (positive implies growth and negative decay) of the linearized transport equation solved by means of a first-order upwind and forward Euler scheme as a function of the number of parts in which a wavelength is divided (small number indicates a coarse resolution) and the Courant number.

where $A$ is the complex amplitude vector, $k$ [rad/m] the real wavenumber, and $\omega = \omega_r + i\omega_i$ [rad/s] the complex angular frequency. The wave celerity $c = \omega_{r/k}$ and the wave attenuation is $\omega_i$. A positive attenuation implies growth of perturbation and a negative value decay. Substituting Eq. (14) into Eq. (13), we obtain:

$$\omega = \lambda k. \tag{15}$$

We find that a linear wave propagates at a celerity $\lambda$ without attenuation.

Considering the above-mentioned numerical scheme, Eq. (13) can be discretized as:

$$\frac{z_{bi}^{\prime n+1} - z_{bi}^{\prime n}}{\Delta t} + \lambda \frac{\left(z_{bi}^{\prime n} - z_{bi-1}^{\prime n}\right)}{\Delta x} = 0, \tag{16}$$

where the indices $i$ and $n$ indicate space and time, respectively. Substituting the wave-like solution (Eq. (14)) into Eq. (16) we find:

$$e^{i(kx-\omega(t+\Delta t))} - e^{i(kx-\omega t)} + \sigma e^{i(kx-\omega t)} - \sigma e^{i(k(x-\Delta x)-\omega t)} = 0, \tag{17}$$

where $\sigma = \lambda \Delta t / \Delta x$ [-] is the Courant number. From this equation we derive:

$$\omega = \frac{i}{\Delta t} \log \left(1 - \sigma + \sigma e^{-ik\Delta x}\right). \tag{18}$$

Fig. 2 shows the attenuation coefficient (i.e., the imaginary part of Eq. (18)) as a function of the number of parts in which a unitary wavelength of $2\pi$ is divided $n = 2\pi/k$, and of the Courant number $\sigma$. The number of parts in which a wavelength is divided indicates the coarseness of the grid. A small number implies that a wavelength is poorly reproduced (i.e., a coarse grid). For a Courant number equal to 1, regardless of the grid resolution, the attenuation coefficient is 0 and the exact solution is recovered. For a Courant number larger than 1, the numerical scheme is unstable, which is seen in the positive attenuation coefficient. For values of the Courant number between 0 and 1, a coarse mesh (less divisions of a wavelength) causes a larger attenuation coefficient than a fine mesh (more divisions of a wavelength).

The artificial diffusion introduced by $F_{TBS}$ adds to the numerical diffusion depending on the discretization or mesh resolution, with different impacts on the final simulated processes. An example on the interlink between $F_{TBS}$ and mesh resolution is given in Section 3.1.2.

### 3.1.2. Two-dimensional considerations

An obvious reason for exaggerating the bed slope effect in morphodynamic computations is the poor representation of steep slopes on a coarse grid. If the numerical representation $\Delta h/\Delta y$ of a transverse bed slope is too small due to a large transverse grid cell size $\Delta y$, the corresponding correction factor must be incorporated in the parameter weighing the effect of gravity pull along transverse bed slopes. This will be investigated in Section 3.1.3 on the basis of numerical simulations.
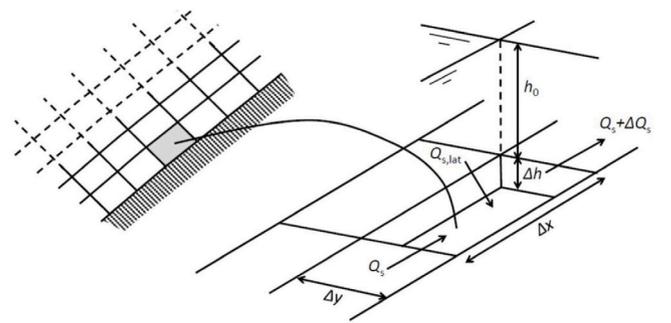


**Fig. 3.** Schematic of mass balance in a coarse-grid situation.

However, there is a second consideration for the need to exaggerate the bed slope effect (i.e., use a smaller value of $f$) if the grid is coarse, related to the stability of the numerical computations, reviewed in the following section.

Assume a 2D computational grid for a river with a horizontal bed and a uniform water depth $h_0$. The river is so wide that the water level is not affected if a single streamwise row of grid cells becomes deeper and thereby locally conveys a higher discharge. So, the water level is constant. Consider the situation in which one grid cell is lowered by $\Delta h$. This enhances the sediment transport capacity by $\Delta Q_s$ and creates a transverse bed slope $\Delta h/\Delta y$, generating a lateral sediment input $\Delta Q_{s,lat}$ (Fig. 3). Neglect backwater effects, so that the flow remains steady and uniform in every grid cell (strongly violating the real flow equations for the sake of a simple analysis).

The bed is stable (self-restoring) if the increase in sediment transport capacity, moving more sediment out of the grid cell than is coming in, is compensated by the lateral input of sediment. This condition can be elaborated as follows, using $Q_s = q_s \Delta y$ and $Q_{s,lat} = q_{s,lat} \Delta x$:

$$\frac{d(q_s \Delta y)}{dh} < \frac{d(q_{s,lat} \Delta x)}{dh} \tag{19}$$

With $q_{s,lat} = \frac{1}{f} \frac{\Delta h}{\Delta y} q_s$ this leads to

$$\Delta y \frac{dq_s}{dh} < \Delta x \frac{q_s}{f} \frac{d}{dh} \left(\frac{\Delta h}{\Delta y}\right) + \Delta x \frac{1}{f} \frac{\Delta h}{\Delta y} \frac{dq_s}{dh} \tag{20}$$

For convenience we introduce the notation $\alpha = \frac{h}{q_s} \frac{dq_s}{dh}$. For a power-law dependence of sediment transport capacity on flow velocity with exponent $b$ and the Chézy equation for steady uniform flow, this parameter is equal to $\alpha = b/2$. It leads to

$$\Delta y \alpha \frac{q_s}{h} < \Delta x \frac{q_s}{f} \frac{d}{dh} \left(\frac{\Delta h}{\Delta y}\right) + \Delta x \frac{1}{f} \frac{\Delta h}{\Delta y} \alpha \frac{q_s}{h}. \tag{21}$$
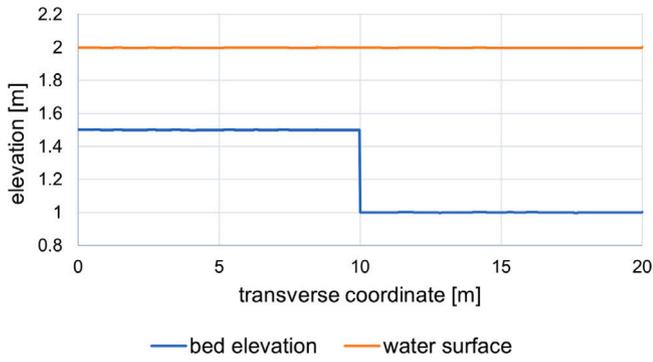
**Fig. 4.** Transverse profile (at coordinate $x = 200\,\mathrm{m}$) of the bed elevation [m] and water surface [m] at the beginning of the simulation.
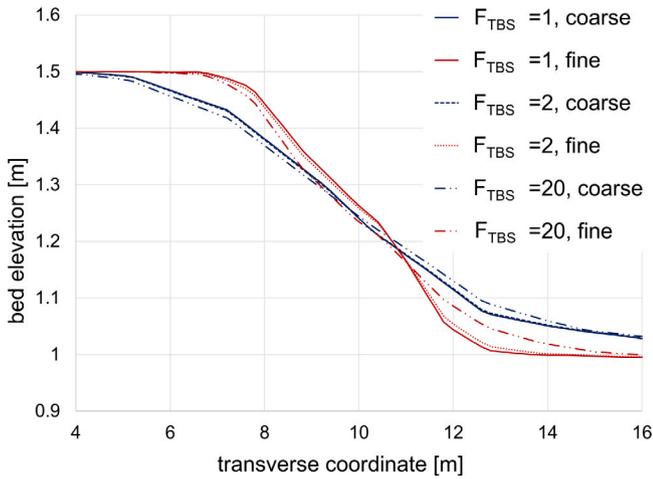


**Fig. 5.** Transverse profile (at coordinate $x = 200\,\mathrm{m}$) of the final bed elevation with two different mesh resolutions (coarse-fine) and three values of $F_{\mathrm{TBS}} = [1, 2, 20]$.

Hence,

$$f < \frac{\Delta x}{\Delta y}\left[\frac{h}{\alpha}\frac{\mathrm{d}}{\mathrm{d}h}\left(\frac{\Delta h}{\Delta y}\right) + \frac{\Delta h}{\Delta y}\right] = \frac{\Delta x}{\Delta y^2}\left(\frac{h}{\alpha} + \Delta h\right) \tag{22}$$

For $\Delta h \ll h$ this reduces to

$$f < \frac{\Delta x}{\Delta y^2}\frac{h}{\alpha}, \tag{23}$$

or for square grid cells

$$f < \frac{1}{\alpha}\frac{h}{\Delta x}. \tag{24}$$

This condition is always fulfilled in the continuum limit as $\Delta x \to 0$. It requires exaggeration of the bed slope effect (i.e., reduction of $f$), however, if $\Delta x > h/\alpha f$.

### 3.1.3. Example: Effect of grid refinement

The effect of grid refinement together with the use of different values of $F_{\mathrm{TBS}}$ is shown via the following numerical test. The computational domain is defined by a rectangular flume [$20\,\mathrm{m} \times 400\,\mathrm{m}$], with lateral vertical frictionless walls. The bottom slope is constant and equal to 0.005. The bottom is divided longitudinally into two flat sections, characterized by a sharp step of $0.5\,\mathrm{m}$ connecting them at the centre line of the channel (Fig. 4). To explore also the role of the mesh resolution, two computational meshes, coarse (3k cells) and fine (13k cells) are used. The Manning value is set to $0.028\,\mathrm{s}\,\mathrm{m}^{-1/3}$ and the inflow to $33.2\,\mathrm{m}^3\mathrm{s}^{-1}$, resulting in a steady flow of approximately $0.5\,\mathrm{m}$ and $1\,\mathrm{m}$ depth on the two sections of the channel, respectively. Simulation time is set to $10\,000\,\mathrm{s}$. These numerical runs were conducted with the
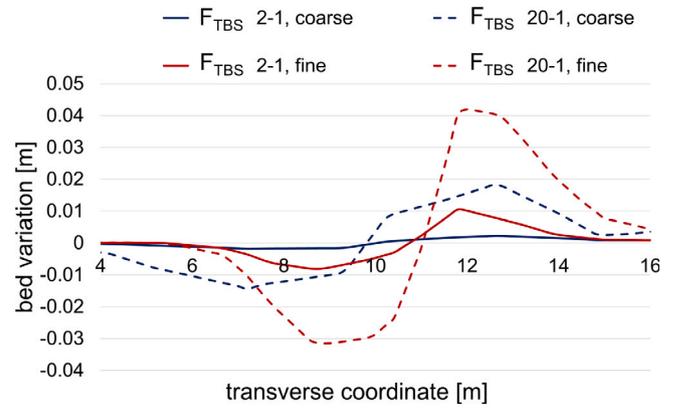


**Fig. 6.** Difference of transverse profiles (at coordinate $x = 200\,\mathrm{m}$) of the final bed elevation between various $F_{\mathrm{TBS}}$ values and for two different mesh resolutions (coarse-fine).

BASEMD module of BASEMENT (Vetsch et al., 2023; ETH Zurich, VAW, 2024).

Fig. 5 shows the bed elevations for two mesh refinements (coarse-fine) and three lateral transport factors ($F_{\mathrm{TBS}} = 1, 2, 20$). The example of Fig. 5 highlights how an increment of $F_{\mathrm{TBS}}$ results, coherently, in an increased diffusion of the bottom step. However, it also clearly emphasizes how the mesh size plays a relevant role in regulating the diffusion of the solution.

Fig. 6 shows the variation of the solution (i.e., difference of bed elevation) when changing $F_{\mathrm{TBS}}$, for both coarse and fine mesh. It is worth noting how $F_{\mathrm{TBS}}$ plays a minor role with a coarse mesh (variation from 1 to 2), hence requiring a larger value to appreciate a difference in the numerical solution (variation from 1 to 20). On the other hand, a finer mesh (i.e., reduced numerical diffusion) results in a higher sensitivity of the numerical solution to the choice of $F_{\mathrm{TBS}}$.

Overall, the test exemplifies how the choice of $F_{\mathrm{TBS}}$ is tightly linked to the mesh resolution, and that the relative effects of varying $F_{\mathrm{TBS}}$ depend on the underlying computational mesh characteristics.

### 3.2. Mesh type and flow orientation

Mesh type (i.e. structured vs unstructured) and flow orientation have well recognized direct effects on numerical diffusion (Patel et al., 1988), and still challenge CFD model developers (e.g Holleman et al., 2013; Bailey, 2017; Green et al., 2022). The use of unstructured grids in hydro-morphodynamic modelling has widely recognized advantages (e.g. easier description of complex geometry and local refinement) but also drawbacks (e.g. more complex implementation and acceleration of numerical solutions). Unstructured meshes have no preferential orientation with respect to the simulated vector field, i.e. an isotropic behaviour with respect to advective and diffusive fluxes. On the contrary, structured meshes have a preferential orientation, i.e. an anisotropic behaviour. A mesh is more anisotropic when it has clearer preferential directions such as for the cases of curvilinear meshes, Cartesian meshes, or meshes using only equilateral triangles.

For the sake of clarity, it is important to distinguish between the numerical solver requirements and the mesh type. Some numerical algorithms are based on the structure of the mesh: for instance, the ADI algorithm (Leendertse, 1967; Briley and McDonald, 1977) in Delft3D 4 requires a curvilinear grid. Other solvers do not require any particular mesh structure, such as in the case of Delft3D Flexible Mesh, BASEMENT (Vanzo et al., 2021; Vetsch et al., 2023) or iSed (Tritthart et al., 2011). This allows covering the domain with triangles of different shapes, leading to an isotropic computational discretization.

One of the main consequences related to the mesh type is that the use of unstructured meshes results in increased numerical diffusion when compared to structured grids well oriented with the

flow field (Holleman et al., 2013). On the contrary, mesh anisotropy (i.e., structured) can reduce numerical diffusion, but it might also reduce physical diffusion by suppressing lateral exchanges, in this case the deviation of the sediment transport vector due to lateral slope.

### 3.2.1. Example: isotropic vs anisotropic mesh

The setup is analogous to the one in 3.1.3. Simulations are conducted with Delft3D Flexible Mesh. The domain is rectangular and it features a straight channel $400\,\mathrm{m}$ long and $20\,\mathrm{m}$ wide with constant streamwise slope equal to $1.6 \times 10^{-3}$ and a step in transverse direction of $0.5\,\mathrm{m}$ separating a floodplain from the main channel. Flow occurs initially only along the $10\,\mathrm{m}$ wide main channel and is in equilibrium for an upstream discharge equal to $4.5\,\mathrm{m}^3\mathrm{s}^{-1}$ and a non-dimensional friction coefficient equal to 0.007 (Chézy friction coefficient equal to $37.44\,\mathrm{m}^{1/2}\mathrm{s}^{-1}$), yielding a normal flow depth equal to $0.45\,\mathrm{m}$. The downstream water level is initially $0\,\mathrm{m}$ and the downstream bed level $-0.45\,\mathrm{m}$. Sediment transport is computed with the relation by Engelund and Hansen (1967) considering the sediment size to be $1\,\mathrm{mm}$. The bed slope effect is modelled according to Koch and Flokstra (1981). This means that the sediment transport vector is rotated in the direction of the bed slope by a certain factor (Eq. (3)). A value of $A = 1$ (Eq. (4)) is employed, which is a physically realistic value (i.e., $F_{\mathrm{TBS}} = 1$). Degradational conditions are imposed by lowering the downstream water level at a rate of $0.5\,\mathrm{m}$ in $30\,\mathrm{days}$. The upstream bed level is lowered at the same rate to simulate the conditions of a long degradational reach. The simulation runs for $12.5\,\mathrm{days}$. Bank erosion is active. The model for bank erosion in Delft3D consists of spreading a fraction of the erosion that would occur in one cell of the main channel (i.e., where there is sediment transport) to the nearby cells if these are higher and there is no sediment transport (i.e., it is a bank). The factor is set to half.

Four different meshes are employed: (1) a Cartesian mesh with square cells of $1\,\mathrm{m}$ side length, (2) a Cartesian mesh with square cells of $2\,\mathrm{m}$ side length, (3) a regular grid with triangles of base equal to $2\,\mathrm{m}$ and height equal to $2\,\mathrm{m}$ (and half these triangles at the open boundaries), and (4) an irregular triangular grid created using the boundaries of Mesh 3. The intention is that Mesh 2, 3, and 4 are of similar resolution, only changing the isotropy characteristics. Nevertheless, the use of triangles of similar size as quadrilaterals inevitably leads to more cells. While we employ 2000 squares for Mesh 2, there are 4010 regular triangles. The grid irregularity also leads to more elements (7174 cells). Mesh 1 is considered to be a reference, given that the Cartesian mesh is expected to be less diffusive (with a well aligned flow), and it has the finest resolution.

Fig. 7 shows the flow depth at the end of the runs for the four meshes. The solution of the high-resolution Cartesian mesh is given in Fig. 7a. For the sake of clarity, let us first compare the results with Mesh 2, 3, and 4 (Fig. 7b, c, and d, respectively), as the result of only varying the mesh type. The solution develops a pronounced meandering channel on a Cartesian mesh (Fig. 7b) whereas the triangular meshes (panel c and d) lead to more uniform bank erosion.

A regular triangular mesh is more isotropic than a Cartesian mesh: Fig. 7c shows a more uniform erosion of the floodplain (compared with panel b), with no meandering pattern visible in the main channel. As somehow expected, the increased isotropy of the regular triangular mesh leads to an increase of the numerical diffusion of the solution, not compensated here by the relative increase of computational cells. A practical workaround to obtain similar results would be to increase the transverse bed slope effect of the Cartesian mesh to increase the lateral diffusion of sediment and prevent the formation of the narrow meandering channel of Fig. 7b.

The irregular triangular mesh (Fig. 7d) is the most isotropic among the tested types: we expect a larger numerical diffusion (due to the mesh type), partially compensated by the increased number of computational cells. Results show an almost homogeneous bank erosion of reduced intensity compared to the regular triangular mesh (Fig. 7c).

Moreover, some pattern of deep and shallow areas in the main channel are also visible.

The simulation results (Fig. 7b to d) show how, for a given factor of lateral transport $F_{\mathrm{TBS}}$: (i) the solution depends on the mesh type and flow alignment, and (ii) it is mediated by the number of computational cells.

The question arises as to which solution is the most correct. As mentioned before, Mesh 1 could be expected to yield the most accurate solution. While numerical diffusion is less than the other grid type, the excessive anisotropy (i.e., clear preferential orientation) could however play a counteracting role.

The high-resolution Cartesian mesh (Fig. 7a) shows results supposedly more diffused than the low-resolution Cartesian mesh (Fig. 7b); the results of the high-resolution Cartesian grid are somewhere in between the triangular meshes and the low-resolution Cartesian grid. Low resolution in a Cartesian mesh (Fig. 7b) causes less diffusion than physically realistic (i.e., flow concentrates in a channel). This shows that mesh resolution should be high enough to prevent flow concentrating in a channel.

Eventually, assuming the most accurate result is obtained with the high-resolution-Cartesian mesh, we conclude that the triangular meshes are too diffusive whilst the low-resolution-Cartesian mesh is too little diffusive. We however refrain from suggesting a conclusive approach to choose the mesh type and granularity. In this exercise the finest-possible Cartesian mesh is considered as most accurate, but this is not true in general. The reason unstructured meshes exist is that these fit better general domains as used in practice.

Our suggestion would be to use a Cartesian or curvilinear mesh if this suits the problem. If the spatial scale varies significantly in the domain of interest (requiring local mesh refinements) or the boundaries cannot be well captured with a curvilinear approach, or if there are islands or bifurcations and confluences which make it difficult to create a good curvilinear mesh, an unstructured mesh should be pursued, as it will reduce the number of cells and the time needed to create it.

If using a Cartesian (or curvilinear) mesh (i.e., with high anisotropy), the resolution needs to be high enough to prevent "underdiffusion". Once the flow concentrates in a few cells, the resolution is not high enough and the mesh should be refined. On the other hand, if using an unstructured mesh (i.e., with low anisotropy), the resolution needs to be high enough to prevent "overdiffusion". When the solution appears too smooth, it is probable that the mesh resolution is not high enough and the mesh should be refined. In essence, creating a suitable mesh is thus still a difficult problem requiring attention and, ideally, iterations and convergence tests.

### 3.3. Numerical scheme and stability of solution algorithm

The advective component of the Exner equation implies that there is a direction in which information travels at a certain celerity. This needs to be considered in the choice of the numerical scheme. Considering the decoupled system of equations (i.e., flow is solved as if the bed is fixed) and vice versa (Colombini and Stocchino, 2005) at the linear level, any downwind component in the numerical solution introduces numerical instability. As such, upwind schemes are a preferred choice, in which the sediment transport direction is used to find the direction.

However, as shown by Volp et al. (2016), this is not always satisfactory. While the two directions (i.e., the bed celerity and the sediment transport) are identical in subcritical 1D models, this is not necessarily the case in 2D and 3D models. Considering an uneven bed with local shallow areas (e.g. due to bed forms or other obstacles), flow can effectively bypass these areas and result in reduced flow velocities on their top. In such a situation, the direction of the bed celerity is different from the sediment transport direction and may even oppose it (Volp et al., 2016).

If the upwinding of the numerical scheme is performed in the wrong direction, what is supposed to be upwind turns out to be downwind,
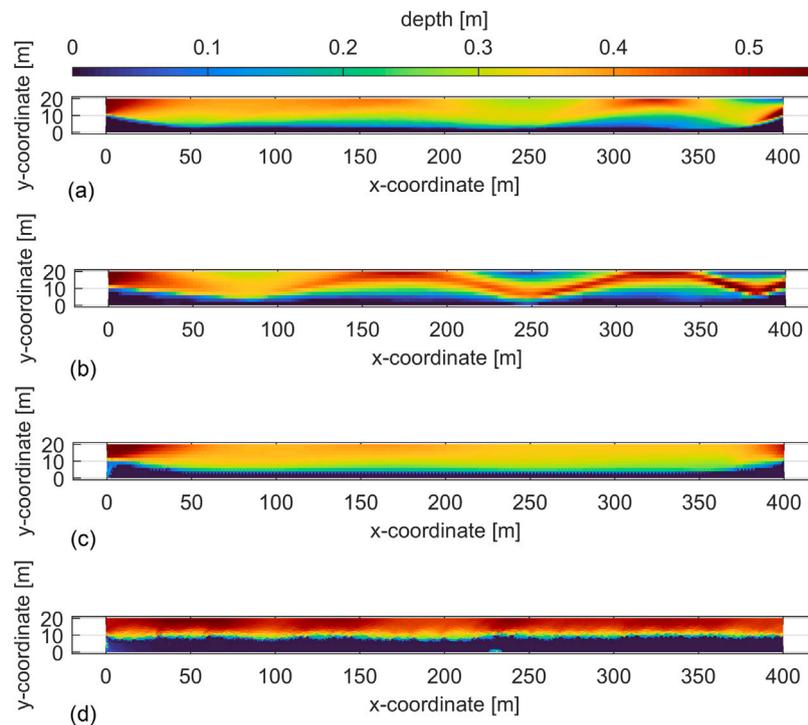
**Fig. 7.** Flow depth using an (a) high-resolution Cartesian mesh, (b) low-resolution Cartesian mesh, (c) regular triangular mesh, (d) irregular triangular mesh.

which causes instability of the numerical scheme. In such a case, artificial damping of the solution is required by adding diffusion, which can be achieved through the bed slope effect by increasing $F_{TBS}$ as already shown mathematically in Section 2.

The problem of an unstable numerical scheme requiring additional diffusion to artificially stabilize it is exacerbated by the use of a morphodynamic acceleration factor (Lesser et al., 2004; Ranasinghe et al., 2011) for reducing the computational time. This factor linearly increases the bed celerity (Carraro et al., 2018) approaching it to the flow celerity travelling downstream. If these are of the same order of magnitude, decoupling of the system of equations is invalid. The bed cannot be assumed to be fixed when solving for the flow and vice versa. The coupled interaction between flow and bed needs to be considered in the solution of the system of equations. In this case, applying an upwind scheme for the Exner equation is unstable, as there is substantial bed information travelling both upstream and downstream. Hence, the application of a pure upwind scheme will be unstable and additional diffusion by means of, for instance, a large $F_{TBS}$ will regularize the system.

## 4. Aspects related to the compensation for unimplemented physical processes

### 4.1. Bank erosion

Bank retreat by erosion is a key process controlling morphodynamic development. An eroding bank represents a source of sediment to the main channel and an increase in flow width. Planform changes are linked to vertical changes and controlling one has an impact on the other. For instance, a non-erodible bank (e.g., engineered using revetments) prevents planform changes. While a crucial process for accurate morphodynamic modelling, it is known to be difficult to predict accurately (ASCE, 1998a,b). Stecca et al. (2017) discern between the difficulties associated to developing (1) an algorithm embedded in a morphodynamic model and (2) a closure relation that rightly models the physics of bank erosion. For instance, a bank can be identified based on the flow depth, sediment transport, difference in height,

or difference in slope between adjacent cells. Furthermore, the grid resolution limits the bank steepness and the change in elevation for a given eroded mass. A coarse grid can more easily cause stalling of the bank retreat. The strength of a bank depends on a myriad of factors such as vegetation, size of slump blocks, ship waves, cohesive sediment, particle interlocking, groundwater, water level variations, particle size, grain size distribution, and vertical heterogeneity (layering) (e.g. Parker et al., 2011; Vargas-Luna et al., 2018; Duró et al., 2020). The amount of literature available and different modelling approaches reflect the difficulty of the topic (see a recent review by Duró, 2020).

For bank retreat to continue, sediment eroded and deposited at the toe needs to be removed. This can be hampered by a small sediment transport at the toe due to a shallow flow. Gradients in sediment transport in streamwise direction near the bank may lead to erosion of the fallen material. Additionally, sediment transport in transverse direction due to bed slope effects efficiently removes sediment, transporting it towards the main channel. The transverse slope at the bank toe is large after sediment has fallen, increasing the efficiency of the process. Transverse sediment transport is ever more important in idealized situations in which quasi-uniform conditions are recreated (i.e., there are limited gradients in streamwise direction).

Compared to the factors involved in bank erosion, the influence of the transverse bed slope on sediment transport appears in first instance to be a less-uncertain process. This fact, in combination with the efficiency of transverse sediment transport in removing sediment from the toe of a bank lets us hypothesize that a large transverse bed slope effect is used to compensate for a poor bank erosion algorithm.

### 4.1.1. Example: Effect on bank erosion

A test case using Delft3D 4 exemplifies how a large bed slope effect enhances bank erosion. The set-up is the same as in Section 3.2 but here the simulation time is 30 days and only a coarse Cartesian grid with square cells of size equal to 5 m is employed. The time step is 1.6 s, guaranteeing that at all time the Courant number (Courant et al., 1928) is below the unstable limit.

Six cases are run varying the bed slope effect. Parameter $A$ (Eq. (4)) is set to 1 (which is a physically realistic value, i.e., $F_{TBS} = 1$), 10, 100,
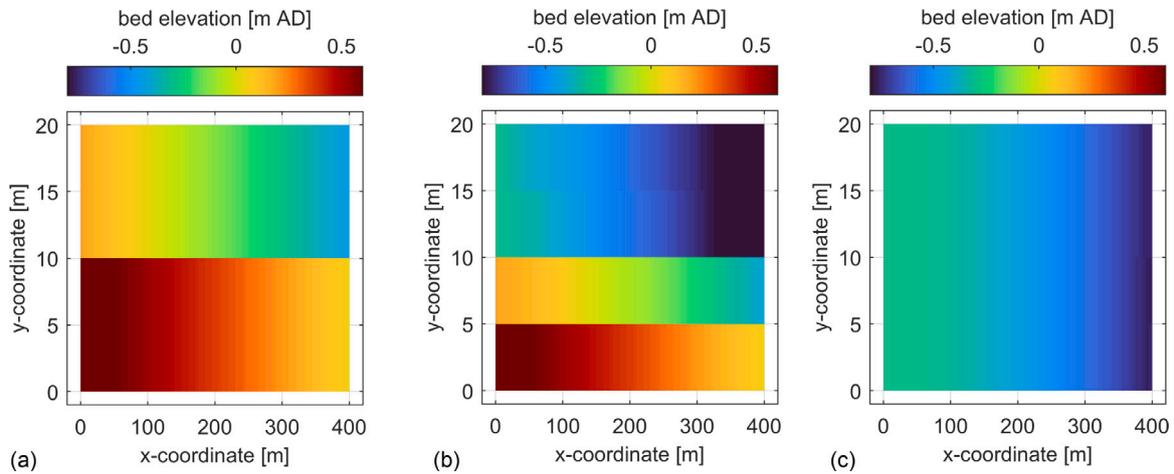
**Fig. 8.** Bank erosion test case, flow from left to right, floodplain on the bottom side; (a) initial bed elevation, (b) bed elevation at the end of the run for a case with $F_{TBS} = 1$ (i.e., physically realistic bed slope effect), (c) bed elevation at the end of the run for a case with $F_{TBS} = 1000$ (i.e., unrealistic bed slope effect).
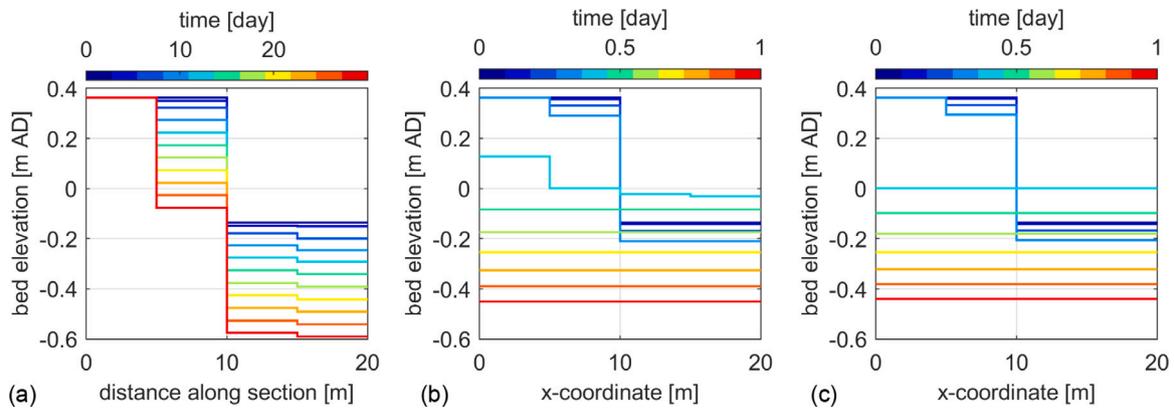


**Fig. 9.** Bed elevation with time along a transverse section at $x = 200$ m (floodplain on the left); for a case with (a) $F_{TBS} = 1$ (i.e., physically realistic bed slope effect), (b) $F_{TBS} = 200$ (i.e., unrealistic bed slope effect), (c) $F_{TBS} = 500$ (i.e., unrealistic bed slope effect).

200, 500, and 1000, respectively. Figs. 8b and 8c show the respective final states for $A = 1$ and $A = 1000$. When a physically realistic value is employed, erosion in the main channel causes bank erosion, but not sufficient to lower the floodplain (Fig. 8b). Fig. 9 shows the development with time along a transverse section at $x = 200$ m, where $x$ is the streamwise direction. When a physically unrealistic value is used, the bed level near the bank is lower, as the sediment is more efficiently transported towards the main channel. The additional erosion causes flow to lower the floodplain, enhancing bank retreat. For $F_{TBS}$ values of up to 100, it does not completely erode the first floodplain cell and for 200 it already erodes the entire floodplain (cf. Figs. 8b and 9b).

### 4.2. Suspended sediment transport

The effect of suspended sediment can be understood from the equilibrium cross-sectional shape that forms in an infinitely long bend of constant curvature. This axisymmetric solution (Struiksma et al., 1985) refers to a hypothetical river spiraling down around a vertical axis (Fig. 10).

The axisymmetric solution for a 2D depth-averaged system is found for the transverse component of sediment transport equal to zero:

$$q_s^* A_s \frac{h}{R} - q_s^{**} \frac{1}{f(\theta)} \frac{\partial z_b}{\partial n} = 0 \qquad (25)$$

where asterisks mark whether the sediment transport rate per unit width is used in the calculation of the effect of helical flow ($q_s^*$) or the effect of transverse bed slopes ($q_s^{**}$); $A_s$ is a factor weighing the effect
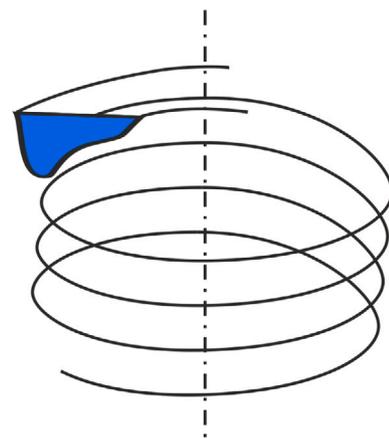


**Fig. 10.** Hypothetical infinitely long riverbend with constant curvature, spiraling down around a vertical axis (pertaining to the axisymmetric solution).

of spiral flow, $h$ the flow depth, $R$ the radius of curvature, and $n$ the transverse coordinate. Hence:

$$\frac{\partial z_b}{\partial n} = \frac{q_s^*}{q_s^{**}} A_s f(\theta) \frac{h}{R} \qquad (26)$$

Unrealistically large values of $\partial z_b / \partial n$ can occur if:

1. the effect of helical flow on sediment transport is calculated as if all suspended sediment is located close to the bed. The parameterization based on equating sediment transport direction to bed shear stress direction is then inappropriate. In the axisymmetric solution this means that $A_s$ is too large (Arailopoulos, 2014; Baar et al., 2019);

2. the effect of transverse bed slope is applied to bedload only, which means that $q_s^{**}$ is taken too small (cf. Eq. (26)). Talmon (1992) found indications that transverse bed slopes affect part of the near-bed suspended sediment transport too.

The occurrence of unrealistically large values of $\partial z_b / \partial n$ is suppressed by making $f(\theta)$ very small during calibration, which is equivalent to exaggerating the bed slope effect (cf. Eq. (7)). If the dispersion by helical flow is modelled inappropriately (i.e., if $A_s$ is taken too large) while applying the bed slope effect to the full suspension (i.e., taking $q_s^{**}$ too large as well), the ratio $A_s/q_s^{**}$ might still be of a realistic order of magnitude so that $f(\theta)$ can have a realistic value too. The model is then calibrated with realistic values for the wrong reasons. This may be what actually happens when applying a total-load predictor such as Engelund and Hansen (1967) to the morphodynamic development of systems with substantial transport in suspension.

## 4.3. Critical bed shear stress

In the development of bed load transport equations, values for critical bed shear stresses were experimentally derived on flat or mildly sloped beds. However, steep slopes, as they are found near banks, in scour holes or the front of sedimentation patches, influence the incipient motion of sediment particles, thus requiring correction of the critical bed shear stress (van Rijn, 1993).

Longitudinal or transverse bed slope effects (e.g. Bagnold, 1966; Ikeda, 1982; Koch and Flokstra, 1981) are applied as a scaling factor to the bedload transport capacity $q_B$. However, $q_B$ is typically derived from threshold equations, such as Meyer-Peter and Müller (1948) or van Rijn (1993), which yield $q_B$=0 if the bed shear stress is below the threshold of incipient motion. During the evolution of a sedimentation patch on an otherwise flat bed, the bed shear stress might drop sharply at the leeward side. In a discretization technique that calculates the bedload transport capacity directly at the cell face without upwinding, e.g. using a staggered mesh where the flow variables are stored in the cell centres and the sediment transport properties at the cell faces, the bedload transport capacity will be zero at the downstream side and non-zero at the upstream side of a cell. This artificially accumulates sediment in a cell, which can become substantially higher than it would be in the physical domain. At this point, the sedimentation front cannot migrate further downstream any more, unless a different discretization technique involving an upwind scheme is employed.

This issue can alternatively be resolved by applying steep-slope corrections for the critical bed shear stress $\tau_{b,cr}$ to the equation set of the modelling framework, such as Smart (1984),

$$\tau_{b,cr} = \tau_{b,cr,0} \left( 1 + \frac{1}{\tan \varphi} \frac{\partial z_b}{\partial s} \right) \tag{27}$$

where $\tau_{b,cr,0}$ is the critical shear stress on a flat bed, $\varphi$ the angle of repose and $s$ the path of the sediment transport vector. These corrections reduce the critical shear stress depending on the bed slope and therefore yield non-zero values of $q_B$ at the leeward side of a sedimentation patch. As the name implies, these corrections were developed for steep-sloped beds and are therefore not necessarily required at the scale of simulation of morphodynamics in rivers or delta regions. However, when morphodynamic features of the bed are accurately represented on a well resolved grid, they are required to obtain a reasonable bed topography. Since these corrections are not available in all modelling frameworks, dampening of the peaks in the sedimentation front otherwise occurring in the numerical solution is required to allow it to migrate downstream. We hypothesize that this can be achieved by exaggeration of the transverse bed slope effect, which effectively introduces enough diffusion that transport becomes possible again.

### 4.3.1. Example: Effect on sediment mobility

In order to test the hypothesis and show the influence of the critical bed shear stress correction on the results, we employ a flume with lateral contraction. We compare model results with and without such a correction to a morphology obtained using an exaggerated transverse slope coefficient.

A physical experiment with the geometry depicted in Fig. 11a was performed by BAW in Germany in the years 2007–2008 (BAW, 2009). The flume was 16.5 m long and 1.0 m wide. 2.93 m downstream of the inlet the flume was narrowed to 0.5 m width by a contraction on the left-hand side, which is 6.88 m long. The vertical side walls of the flume consisted of plastered, smooth concrete. The channel bed had zero slope. Experiments were performed for a duration of $T = 125$ min for various steady-state discharges; we considered the experiment using the maximum discharge of $0.15\,\mathrm{m^3 s^{-1}}$ and an initial downstream water depth of $h_0 = 0.275$ m. A sediment layer of 0.2 m thickness in the flume was characterized by the following grain sizes: $d_{50} = 4.9$ mm, $d_m = 5.1$ mm, $d_{90} = 7.6$ mm and $\sigma = (d_{84}/d_{16})^{0.5} = 1.6$. The dominating fraction was fine gravel with grain sizes between 2.0 mm and 6.3 mm.

In this test case, the iSed sediment code (Tritthart et al., 2011) serves as the numerical model and is fully coupled with the RSim-3D hydrodynamic solver (Tritthart and Gutknecht, 2007). A mesh consisting of cells in quadrilateral base shape, ranging from 0.04 m × 0.02 m to 0.04 m × 0.04 m is used; the mesh is refined near the walls and in the contraction section. Eight cells in the vertical discretize the water column. Bedload transport is computed using the equation by Meyer-Peter and Müller (1948), formulated for non-uniform transport with the hiding-exposure (HE) correction by Einstein (1950). Generic parameters are applied, i.e. $\theta_c = 0.047$ and a HE coefficient of $\gamma_{HE} = -0.5$. The bed slope effect is modelled using the equation by Ikeda (1982) (Eq. (5)) using a standard bed slope factor $\varepsilon = 1.5$ as well as an exaggerated bed slope factor $\varepsilon = 15$, i.e. $F_{TBS} = 10$. The correction of the critical bed shear stress is performed according to Eq. (27) (labelled as *full* $\tau_{b,cr}$ correction) and alternatively limited to the range [0.5, 1.5] $\tau_{b,cr,0}$ (labelled as *weak* $\tau_{b,cr}$ correction).

Fig. 11b presents a longitudinal section of the channel at the end of the experiment. The computation using a standard bed slope factor $F_{TBS} = 1$ and full critical bed shear stress correction shows a smooth behaviour of the morphodynamics in the channel. The sedimentation deposit advances to $x/L = 0.8$. In contrast, the computation with $F_{TBS} = 1$ and disabled critical bed shear stress correction leads to a pronounced sediment deposition in the widening zone of the channel. This deposit forms early in the computations and does not proceed downstream. On the other hand, the simulation using an exaggerated bed slope factor $F_{TBS} = 10$ predicts the deposit to migrate further downstream, to a position of $x/L = 0.7$. In this computation, the front is not immobile and progresses slowly further. Both scour depth and deposition height, however, are larger than in the simulation with full correction of the critical bed shear stress. When a weak (limited) correction of the critical bed shear stress is employed, the deposit migrates further downstream. Using $F_{TBS} = 10$ in this case yields the same result as the computation with the full critical bed shear stress corrections. Thus, an exaggerated transverse bed slope factor can mitigate a deficient correction of the bed shear stress. This behaviour can also be inferred from Eq. (5) where a too small value of $\tau_{b,cr}$ can be compensated by an exaggerated $\varepsilon$ (and thus a larger $F_{TBS}$) to yield the same transverse bed slope effect.

## 5. Discussion

The provided examples have shown that an exaggeration of the transverse bed slope effect using a value of $F_{TBS}$ substantially larger than 1, can either stabilize the numerical solution or compensate for physical processes not implemented in the model, or both. Thereby a "desired" morphological evolution can be achieved more easily. According to our findings, the need to increase the transverse bed slope
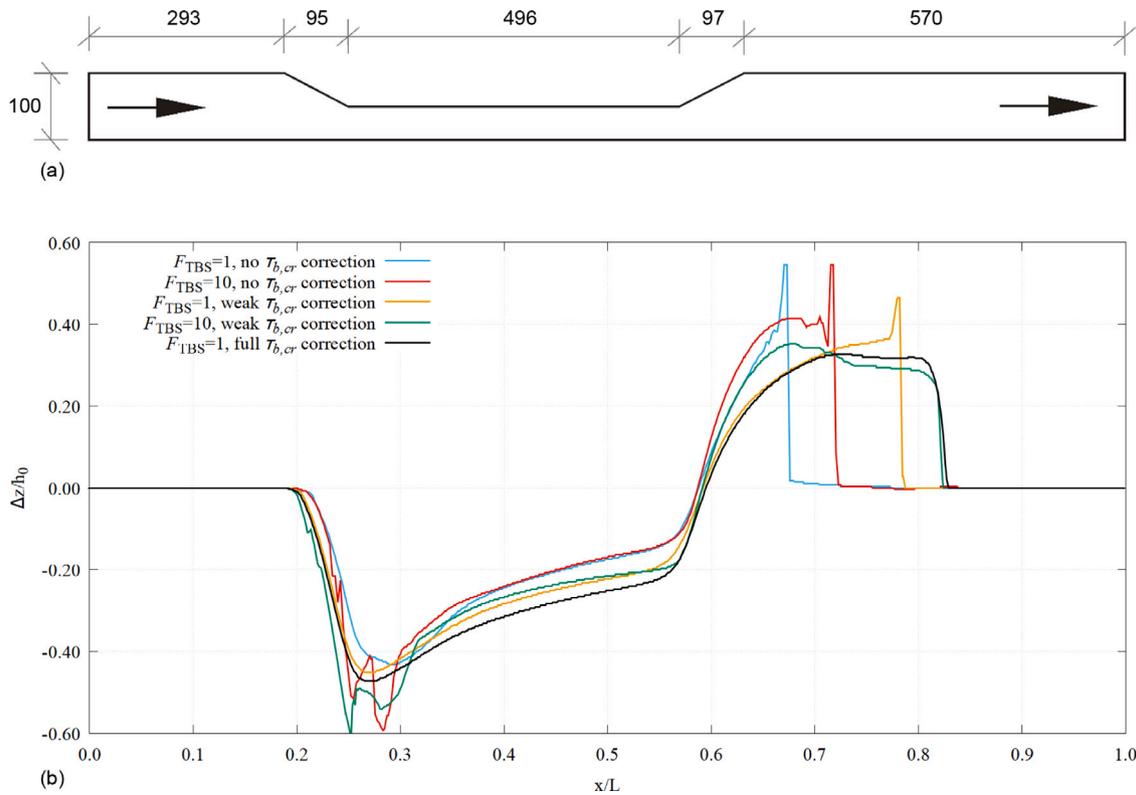
**Fig. 11.** (a) Plan view of the channel constriction experiment with distances in cm; (b) longitudinal section of relative bed level changes with no, weak and full critical bed shear stress correction as well as $F_{TBS} = 1$ and increased $F_{TBS} = 10$.

effect to unrealistic values therefore does not arise from a preference of the water to flow through as few grid cells as possible, as suggested by Baar et al. (2019), but rather to overcome other deficiencies of the modelling framework employed.

Empirical relationships to calculate bedload transport capacities were typically derived for flat beds. Approaches to consider the bed slope effect are generally required to increase or decrease the bedload transport capacities accordingly to match the actual slopes encountered (cf. Sections 2 and 4.3). However, depending on the situation these terms may add substantial diffusion to the numerical solution. This is the case particularly for comparably steep slopes. For instance, longitudinal bed slope equations following the approach by Bagnold (1966), may increase the bedload transport capacity by the order of $10^3$ for slopes near the value of the inner friction angle of the sediment. While this may be true for an "avalanche" process, which takes place within time spans of seconds, it obviously acts destabilizing on the numerical solution of larger domains with longer simulation time steps. The general failure of the (Bagnold, 1966) hypothesis as discussed by Seminara et al. (2002) notwithstanding, this approach is widely used. The introduction of slope correction terms of the critical bed shear stress, such as those suggested by Smart (1984) and presented in the example in Section 4.3, have a stabilizing effect in such situations by dampening potentially large values. Again, from a numerical point of view this works by adding diffusion to the solution. Without the availability of such a correction in the model, an exaggerated $F_{TBS}$ provides an alternative remedy.

However, exaggerating the transverse bed slope effect for targeting the aforementioned aims does not come without severe "side effects", as additional diffusion in the numerical solution may suppress – or even reverse – physical processes that would otherwise be correctly predicted by the model. In the following example, we show what happens to a self-formed river morphology under an exaggerated $F_{TBS}$ scenario.
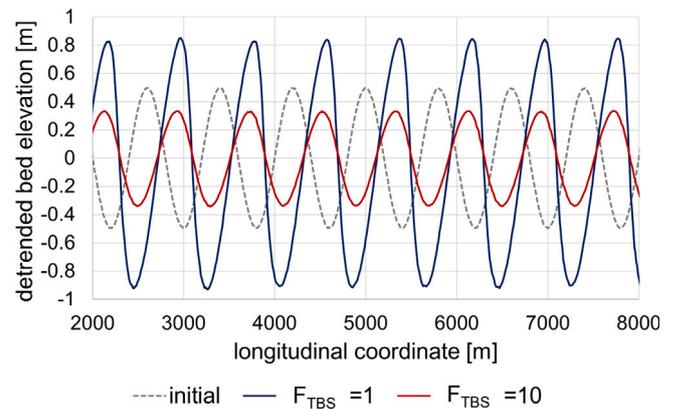


**Fig. 12.** Longitudinal profile of the detrended bed elevation at the channel side wall ($y = 0$). Dashed grey line is the initial bed profile for the simulations, whilst blue and red lines are the final profiles ($t = 1d$) with $F_{TBS} = 1$ and $F_{TBS} = 10$, respectively.

## 5.1. Example: Effect of $F_{TBS}$ on self-formed river morphology

The computational domain is composed by a straight channel [100 m × 10 000 m] characterized by a constant slope of 0.002, discretized with 42674 computational cells, and having frictionless vertical lateral walls. The initial bottom is modulated with a periodic cosine-sinusoidal undulation, with a half-period in the transverse direction. The amplitude of the signal is 1 m, whilst the wavenumber is set to 0.4. The initial conditions of the bed resemble an alternate bar configuration.

The bottom is assumed to be composed by uniform sediment having a representative diameter of 0.02 m and a relative submerged mass density of 1.65. The bottom friction is set to $30 \, \text{m}^{1/3} \, \text{s}^{-1}$ (Strickler
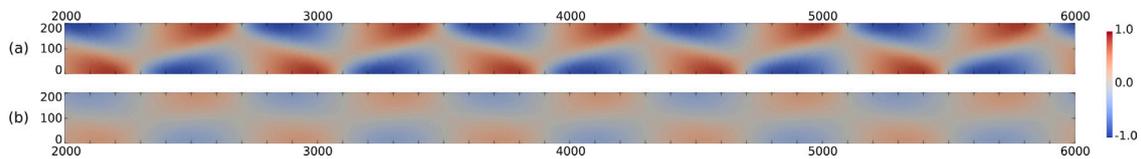
**Fig. 13.** Planar view of detrended bed variation [m] at final time $t = 1d$. Axes are distorted and flow is from left to right. Starting from the same initial conditions, simulation (a) $F_{TBS} = 1$ shows a growing pattern of alternate bars, whilst simulation (b) $F_{TBS} = 10$ shows a decaying signal, towards a morphological equilibrium characterized by flat-bed conditions.

parameterization) and the sediment transport is evaluated with the formula of Meyer-Peter and Müller (1948). The system is fed with a constant water discharge of $1000\,\mathrm{m^3 s^{-1}}$ and a sediment discharge in equilibrium with the actual inlet transport capacity. With the provided boundary conditions, the domain is subject to sediment transport everywhere, with an average Shields stress of 0.2.

With the provided hydro-morphological conditions, the expected equilibrium self-formed morphology is represented by free migrating alternating bars, consistently predicted by Colombini et al. (1987). Thus, the numerical solution is expected to represent a growing and downstream travelling signal. The simulation time is set to 1 day and the simulations are executed with the BASEMD module of BASEMENT (Vetsch et al., 2023; ETH Zurich, VAW, 2024).

Fig. 12 shows the longitudinal profiles of the initial bed and the final results, for both cases of $F_{TBS} = 1$ and $F_{TBS} = 10$. Coherently with the bar predictor approaches of Colombini et al. (1987) and Crosato and Mosselman (2009), the regular case of $F_{TBS} = 1$ results in a growing signal of the bars. While growing, the initial sinusoidal signal also evolves towards an alternate bar shape, with more pronounced head and milder tail of the depositions, as shown in Fig. 13a. On the contrary, with an exaggerated $F_{TBS} = 10$, the morphodynamic evolution of the system is reversed. Despite the expected self-formed morphology as alternate bars, the initial bottom tends to flatten as effect of the strong diffusion introduced with $F_{TBS}$. The initial signal hence decays almost symmetrically (Fig. 13b), ultimately leading to a flat-bed equilibrium condition.

The test exemplifies how the tuning-exaggeration of $F_{TBS}$ can lead to a complete reversal of expected morphodynamic processes. When modelling such physically rooted morphodynamic processes, it is therefore not recommended to scale the bed slope factor to more than the value range actually tested by the original authors of the approach (e.g. $F_{TBS}$ 1 to 2 in the case of a transverse bed slope implementation of the van Bendegom (1947) type (cf. Eq. (3)), such as Koch and Flokstra, 1981 or Talmon et al., 1995).

## 6. Conclusions

Through mathematical analysis and five examples, we show that the main reasons for using unrealistic representations of the bed slope effect in morphodynamic modelling are (i) the need for stabilizing the numerical solution through added diffusion, and (ii) the compensation of missing physical processes in the model implementation. In detail, practical reasons for employing an increased bed slope effect are:

- compensating an insufficient resolution or isotropy of the numerical mesh;
- stabilizing and smoothing the numerical solution, in particular due to an inappropriate choice of the numerical scheme;
- substituting a lacking or oversimplified bank erosion algorithm;
- coping with too simple model approaches of suspended sediment transport processes;
- mitigating the lack of a slope correction of the critical bed shear stress.

There is no reason to conclude that realistic sediment transport vectors and realistic transverse bed slope effects cannot coexist in the same model study. If in the context of a practical model application

an improved result is only obtained through a substantially increased transverse bed slope factor, the resolution of the numerical mesh and the appropriateness of the numerical scheme should be checked first. Then, the processes implemented in the model should be matched with those physically occurring in prototype conditions. Only if all of these influences can be excluded, a tweaking of the transverse bed slope factor should be considered. However, even under these circumstances we do not recommend changing this factor by more than twice its default value, as this is the proven value range found in the original literature of the transverse bed slope effects. Employing larger values bears the substantial risk of a strong alteration and even reversal of physically expected morphodynamic processes.

## Potential conflicts of interest

As developers of different modelling systems (BASEMENT, Delft3D, RSim-3D and iSed), the authors do not favour a particular software. The findings here presented are to be considered generic and do not depend on any specific software system.

## CRediT authorship contribution statement

**Michael Tritthart:** Writing – review & editing, Writing – original draft, Visualization, Supervision, Software, Methodology, Investigation, Formal analysis, Data curation, Conceptualization. **Davide Vanzo:** Writing – review & editing, Writing – original draft, Visualization, Software, Methodology, Investigation, Formal analysis, Data curation, Conceptualization. **Victor Chavarrías:** Writing – review & editing, Writing – original draft, Visualization, Software, Methodology, Investigation, Formal analysis, Data curation, Conceptualization. **Annunziato Siviglia:** Writing – review & editing, Investigation, Formal analysis. **Kees Sloff:** Writing – review & editing, Investigation. **Erik Mosselman:** Writing – review & editing, Writing – original draft, Visualization, Methodology, Investigation, Formal analysis, Conceptualization.

## Declaration of competing interest

The authors declare the following financial interests/personal relationships which may be considered as potential competing interests: Editorial board member of Advances in Water Resources - Annunziato Siviglia (co-author). If there are other authors, they declare that they have no known competing financial interests or personal relationships that could have appeared to influence the work reported in this paper.

## Acknowledgments

## Appendix. Software used

In this section, the software employed in this manuscript is briefly described.

*Delft3D.* Delft3D 4 (Deltares, 2024b) and Delft3D Flexible Mesh (Deltares, 2024a) are both products of Deltares. Delft3D 4 requires a curvilinear mesh. The numerical scheme is staggered and based on finite differences. An Alternate Implicit Direction scheme (Leendertse, 1967; Briley and McDonald, 1977) efficiently and accurately solves the flow with Courant numbers of up to 5–10 in practical applications.

Delft3D Flexible Mesh solves on unstructured orthogonal meshes composed of elements of up to 6 sides (i.e., hexagons, although usually triangles and quadrilaterals are employed, and some pentagons for joining subgrids). The numerical scheme is staggered and based on finite volumes. A semi-implicit scheme is employed, which sets the time-step limit to a Courant number based only on flow velocity, smaller than 1. In other words, the time step is limited by $u$ and not by $u + \sqrt{gh}$.

The morphodynamic component of Delft3D 4 and Delft3D Flexible Mesh is the same (both share the same source code). The bed level is defined at cell centres and considered piece-wise constant (i.e., tile approach). The fluxes are determined by upwinding the sediment transport computed at cell centres. The bed level update is computed decoupled from the flow update. In other words, the flow is assumed to weakly interact with the bed, such that the flow can be considered constant for updating the bed level and vice-versa.

*Basement.* It is a freeware application developed at the Laboratory of Hydraulics, Hydrology and Glaciology of ETH Zürich. The software can simulate two-dimensional hydrodynamic, morphodynamic, and scalar advection-diffusion processes of scientific and practical interest (Vanzo et al., 2021). For the test cases of this work we employed the BASEMD module of the software (Vetsch et al., 2023).

BASEMENT solves the 2D hydro-morphodynamic governing equations (shallow water and Exner) adopting a finite volume approach over unstructured triangular meshes. The computational meshes can be generated with BASEmesh, an open-source Python module, as well as a QGIS plugin Vanzo et al. (2021). For the temporal integration, an explicit first order Euler scheme is used. The temporal integration proceeds in a synchronous-decoupled way for the hydrodynamic (shallow water) and morphodynamic (Exner) equations, meaning that the modules are independently integrated in time with the same timestep.

In the BASEMD module, hydrodynamic fluxes are calculated with an HLLC solver on the main triangular mesh, whilst the morphodynamic fluxes are calculated with an upwind approach on a staggered grid, resulting in a sediment flux estimation at the cell interface of the main triangular mesh. For more details refer to the official documentation (https://basement.ethz.ch/https://basement.ethz.ch/).

*RSim-3D.* Short for *River Simulation in 3D*, the code uses a generalized finite volume method (Tritthart and Gutknecht, 2007) to solve the three-dimensional Reynolds-averaged Navier–Stokes equations on arbitrarily shaped polyhedra. The solver employs a second-order upwind scheme for convective fluxes and a central differencing scheme for diffusive fluxes. Temporal integration is performed using an explicit first order Euler scheme. Turbulence is modelled using a two-equation closure (user-selectable $k$-$\epsilon$ or $k$-$\omega$). The position of the free surface is computed from the non-hydrostatic pressure field, which is coupled with the velocity field via the SIMPLE algorithm. While RSim-3D contains code to calculate suspended sediment transport in 3D (cf. Tritthart et al., 2019b), it does not come with capabilities to compute bed load transport processes or morphodynamics by itself.

*iSed.* An abbreviation for *integrated sediment transport and morphodynamics model*, the iSed code (Tritthart et al., 2011) extends 2D and 3D hydrodynamic models by the functionality to compute suspended load, bed load, morphodynamics (Exner equation) and sediment sorting processes. Since version 3.0, iSed uses shared-memory data exchange to obtain the flow properties from the respective hydrodynamic codes and in turn deliver bed level and roughness changes due to morphodynamics. This results in a synchronous-decoupled workflow of hydrodynamic

and morphodynamic calculations, using an explicit first order Euler scheme for the temporal integration. To handle different meshes, it uses the same generalized finite volume method as RSim-3D (Tritthart and Gutknecht, 2007). Morphodynamic fluxes are calculated using an upwind technique on a staggered grid, i.e. while the bed levels are stored in the cell centres, the fluxes are stored on the cell faces of the original mesh of the hydrodynamics solver.

## Data availability

Data will be made available on request.

## References

Arailopoulos, I., 2014. Morphodynamic Modelling with Suspended Sediment Transport in River Bends (Master's thesis). Delft University of Technology.

ASCE, 1998a. River width adjustment. I: Processes and mechanics. J. Hydraul. Eng. 124 (9), 882–902, ASCE Task Committee on Hydraulics, Bank Mechanics and Modelling of River Width Adjustment.

ASCE, 1998b. River width adjustment. II: Modelling. J. Hydraul. Eng. 124 (9), 903–917, ASCE Task Committee on Hydraulics, Bank Mechanics and Modelling of River Width Adjustment.

Ashida, K., Michiue, M., 1971. An investigation of river bed degradation downstream of a dam. In: Proc. of the 14th IAHR World Congress, 29 August–3 September, Paris, France, vol. 3, pp. 247–255.

Baar, A.W., Boechat Albernaz, M., van Dijk, W.M., Kleinhans, M.G., 2019. Critical dependence of morphodynamic models of fluvial and tidal systems on empirical downslope sediment transport. Nature Commun. 10 (1), 4903. http://dx.doi.org/10.1038/s41467-019-12753-x.

Bagnold, R.A., 1966. In: Off., U. S. Govt. Print. (Ed.), An Approach to the Sediment Transport Problem from General Physics. Technical Report, USGS, http://dx.doi.org/10.3133/pp422I.

Bailey, R.T., 2017. Managing false diffusion during second-order upwind simulations of liquid micromixing. Int. J. Numer. Methods Fluids 83 (12), 940–959. http://dx.doi.org/10.1002/fld.4335.

Barneveld, H.J., Mosselman, E., Chavarrías, V., Hoitink, A.J.F., 2023. Can linear stability analyses predict the development of riverbed waves with lengths much larger than the water depth? Water Resour. Res. 59 (3), e2022WR033281. http://dx.doi.org/10.1029/2022WR033281, e2022WR033281 2022WR033281.

Barneveld, H.J., Mosselman, E., Chavarrías, V., Hoitink, A.J.F., 2024. Accuracy assessment of numerical morphological models based on reduced saint-venant equations. Water Resour. Res. 60 (1), e2023WR035052. http://dx.doi.org/10.1029/2023WR035052, e2023WR035052 2023WR035052.

BAW, 2009. Morphologische Versuche an einer Rinne mit Einschnürung, (Morphological Experiments in a Flume with Contraction). Technical Report, BAW, Karlsruhe, Germany.

Bell, R.G., Sutherland, A.J., 1983. Nonequilibrium bedload transport by steady flows. J. Hydraul. Eng. 109 (3), 351–367. http://dx.doi.org/10.1061/(ASCE)0733-9429(1983)109:3(351).

van Bendegom, L., 1947. Eenige beschouwingen over riviermorphologie en rivierverbetering. Ingenieur 59, 1–11.

Blondeaux, P., Seminara, G., 1985. A unified bar-bend theory of river meanders. J. Fluid Mech. 157, 449–470. http://dx.doi.org/10.1017/S0022112085002440.

Briley, W.R., McDonald, H., 1977. Solution of the multidimensional compressible Navier–Stokes equations by a generalized implicit method. J. Comput. Phys. 24 (4), 372–397. http://dx.doi.org/10.1016/0021-9991(77)90029-8.

Carraro, F., Vanzo, D., Caleffi, V., Valiani, A., Siviglia, A., 2018. Mathematical study of linear morphodynamic acceleration and derivation of the MASSPEED approach. Adv. Water Resour. 117, 40–52. http://dx.doi.org/10.1016/j.advwatres.2018.05.002.

Chavarrías, V., Schielen, R., Ottevanger, W., Blom, A., 2019. Ill posedness in modelling two-dimensional morphodynamic problems: Effects of bed slope and secondary flow. J. Fluid Mech. 868, 461–500. http://dx.doi.org/10.1017/jfm.2019.166.

Colombini, M., Seminara, G., Tubino, M., 1987. Finite-amplitude alternate bars. J. Fluid Mech. 181, 213–232. http://dx.doi.org/10.1017/S0022112087002064.

Colombini, M., Stocchino, A., 2005. Coupling or decoupling bed and flow dynamics: Fast and slow sediment waves at high Froude numbers. Phys. Fluids 17 (3), 036602. http://dx.doi.org/10.1063/1.1848731.

Courant, R., Friedrichs, K., Lewy, H., 1928. Über die partiellen differenzengleichungen der mathematischen physik. Math. Ann. 100, 32–74, (in German). URL http://eudml.org/doc/159283.

Crosato, A., Mosselman, E., 2009. Simple physics-based predictor for the number of river bars and the transition between meandering and braiding. Water Resour. Res. 45 (3), http://dx.doi.org/10.1029/2008WR007242.

Deltares, 2024a. Delft3D Flexible Mesh Suite. Technical Report, Deltares, Delft, the Netherlands, URL https://content.oss.deltares.nl/delft3dfm2d3d/D-Flow_FM_User_Manual.pdf.

Deltares, 2024b. Delft3D, User Manual. Technical Report, Deltares, Delft, the Netherlands, URL https://content.oss.deltares.nl/delft3d4/Delft3D-FLOW_User_Manual.pdf.

van Dijk, W.M., Hiatt, M.R., van der Werf, J.J., Kleinhans, M.G., 2019. Effects of shoal margin collapses on the morphodynamics of a sandy estuary. J. Geophys. Res.: Earth Surface 124 (1), 195–215. http://dx.doi.org/10.1029/2018JF004763.

Duró, G., 2020. Bank Erosion in Regulated Navigable Rivers (Ph.D. thesis). Delft University of Technology.

Duró, G., Crosato, A., Kleinhans, M.G., Winkels, T.G., Woolderink, H.A., Uijttewaal, W.S., 2020. Distinct patterns of bank erosion in a navigable regulated river. Earth Surf. Process. Landf. 45 (2), 361–374. http://dx.doi.org/10.1002/esp.4736.

Einstein, H., 1950. The Bed-load Function for Sediment Transportation in Open Channel Flows. In: Technical Bulletin (United States. Dept. of Agriculture), U.S. Department of Agriculture.

Engelund, F., Hansen, E., 1967. Monograph on Sediment Transport in Alluvial Streams. Tech. Rep., Hydraulics Laboratory, Technical University of Denmark, Copenhagen, Denmark, p. 63.

ETH Zurich, VAW, 2024. BASEMENT - Basic Simulation Environment for Computation of Environmental Flows and Natural Hazard Simulation. URL https://basement.ethz.ch/.

Exner, F.M., 1920. Zur Physik der Dünen. Akad. Wiss. Wien Math. Naturwiss 129 (2a), 929–952, (in German).

Green, D., Hu, X., Lore, J., Mu, L., Stowell, M.L., 2022. An efficient high-order numerical solver for diffusion equations with strong anisotropy. Comput. Phys. Comm. 276, 108333.

Holleman, R., Fringer, O., Stacey, M., 2013. Numerical diffusion for flow-aligned unstructured grids with application to estuarine modeling. Internat. J. Numer. Methods Fluids 72 (11), 1117–1145. http://dx.doi.org/10.1002/fld.3774.

Ikeda, S., 1982. Lateral bed load transport on side slopes. J. Hydraulics Div., ASCE 108 (11), 1369–1373. http://dx.doi.org/10.1061/JYCEAJ.0005937.

Jain, S.C., 1992. Note on lag in bedload discharge. J. Hydraul. Eng. 118 (6), 904–917. http://dx.doi.org/10.1061/(ASCE)0733-9429(1992)118:6(904).

Koch, F., Flokstra, C., 1981. Bed level computations for curved alluvial channels. In: Proceedings of the 19th IAHR Congress, New Delhi, India. IAHR Congress.

Leendertse, J.J., 1967. Aspects of a Computational Model for Long-Period Water-Wave Propagation. Technical Report RM-5294-RR, Rand Corporation, Santa Monica, CA, United States.

Lesser, G.R., Roelvink, J.A., van Kester, J.A.T.M., Stelling, G.S., 2004. Development and validation of a three-dimensional morphological model. Coastal Eng. 51 (8–9), 883–915. http://dx.doi.org/10.1016/j.coastaleng.2004.07.014.

Marciano, R., Wang, Z.B., Hibma, A., de Vriend, H.J., Defina, A., 2005. Modeling of channel patterns in short tidal basins. J. Geophys. Res.: Earth Surface 110 (F1), http://dx.doi.org/10.1029/2003JF000092.

Meyer-Peter, E., Müller, R., 1948. Formulas for bed-load transport. In: Proceedings of the 2nd IAHR Congress, Stockholm, Sweden. pp. 39–64.

Mosselman, E., Le, T.B., 2015. Five common mistakes in fluvial morphodynamic modeling. Adv. Water Resour. 93(A), 15–20. http://dx.doi.org/10.1016/j.advwatres.2015.07.025.

Nicholas, A.P., Ashworth, P.J., Sambrook Smith, G.H., Sandbach, S.D., 2013. Numerical simulation of bar and island morphodynamics in anabranching megarivers. J. Geophys. Res.: Earth Surface 118 (4), 2019–2044. http://dx.doi.org/10.1002/jgrf.20132.

Parker, G., Shimizu, Y., Wilkerson, G.V., Eke, E.C., Abad, J.D., Lauer, J.W., Paola, C., Dietrich, W.E., Voller, V.R., 2011. A new framework for modeling the migration of meandering rivers. Earth Surf. Process. Landf. 36 (1), 70–86. http://dx.doi.org/10.1002/esp.2113.

Patel, M., Cross, M., Markatos, N.-C., 1988. An assessment of flow oriented schemes for reducing 'false diffusion'. Int. J. Numer. Methods Eng. 26 (10), 2279–2304. http://dx.doi.org/10.1002/nme.1620261011.

Phillips, B.C., Sutherland, A.J., 1989. Spatial lag effects in bed load sediment transport. J. Hydraul. Res. 27 (1), 115–133. http://dx.doi.org/10.1080/00221688909499247.

Ranasinghe, R., Swinkels, C., Luijendijk, A., Roelvink, D., Bosboom, J., Stive, M., Walstra, D., 2011. Morphodynamic upscaling with the MORFAC approach: Dependencies and sensitivities. Coastal Eng. 58 (8), 806–811. http://dx.doi.org/10.1016/j.coastaleng.2011.03.010.

van Rijn, L., 1993. Principles of Sediment Transport in Rivers, Estuaries and Coastal Seas. Aqua Publications.

Schuurman, F., Marra, W.A., Kleinhans, M.G., 2013. Physics-based modeling of large braided sand-bed rivers: Bar pattern formation, dynamics, and sensitivity. J. Geophys. Res.: Earth Surface 118 (4), 2509–2527. http://dx.doi.org/10.1002/2013JF002896.

Seminara, G., Solari, L., Parker, G., 2002. Bed load at low Shields stress on arbitrarily sloping beds: Failure of the Bagnold hypothesis. Water Resour. Res. 38 (11), 31–1–31–16. http://dx.doi.org/10.1029/2001WR000681.

Shields, A., 1936. Anwendung der Ähnlichkeitsmechanik und Turbulenzforschung auf die Geschiebebewegung (Ph.D. thesis). Versuchsanstalt für Wasserbau und Schiffbau, 26, Berlin, Germany, (in German).

Siviglia, A., Crosato, A., 2016. Numerical modelling of river morphodynamics: Latest developments and remaining challenges. Adv. Water Resour. 93, 1–3. http://dx.doi.org/10.1016/j.advwatres.2012.11.010.

Smart, G.M., 1984. Sediment transport formula for steep channels. J. Hydraul. Eng. 110 (3), 267–276. http://dx.doi.org/10.1061/(ASCE)0733-9429(1984)110:3(267).

Stecca, G., Measures, R., Hicks, D.M., 2017. A framework for the analysis of noncohesive bank erosion algorithms in morphodynamic modeling. Water Resour. Res. 53 (8), 6663–6686. http://dx.doi.org/10.1002/2017WR020756.

Struiksma, N., Crosato, A., 1989. Analysis of a 2-D bed topography model for rivers. In: River Meandering. American Geophysical Union (AGU), pp. 153–180. http://dx.doi.org/10.1029/WM012p0153, Chapter 6.

Struiksma, N., Olesen, K.W., Flokstra, C., Vriend, D.H.J.D., 1985. Bed deformation in curved alluvial channels. J. Hydraul. Res. 23 (1), 57–79. http://dx.doi.org/10.1080/00221688509499377.

Talmon, A., 1992. Bed topography of river bends with suspended sediment transport. In: Communications on Hydraulic and Geotechnical Engineering, (No. 92-5), Delft University of Technology.

Talmon, A., Struiksma, N., Mierlo, M.V., 1995. Laboratory measurements of the direction of sediment transport on transverse alluvial-bed slopes. J. Hydraul. Res. 33 (4), 495–517. http://dx.doi.org/10.1080/00221689509498657.

Toro, E.F., 2009. Riemann Solvers and Numerical Methods for Fluid Dynamics. Springer Berlin, Heidelberg, http://dx.doi.org/10.1007/b79761.

Tritthart, M., Gmeiner, P., Liedermann, M., Habersack, H., 2019a. A meso-scale gravel tracer model for large gravel-bed rivers. J. Appl. Water Eng. Res. 7 (2), 89–102. http://dx.doi.org/10.1080/23249676.2018.1449674.

Tritthart, M., Gutknecht, D., 2007. Three-dimensional simulation of free-surface flows using polyhedral finite volumes. Eng. Appl. Comput. Fluid Mech. 1 (1), 1–14. http://dx.doi.org/10.1080/19942060.2007.11015177.

Tritthart, M., Haimann, M., Habersack, H., Hauer, C., 2019b. Spatio-temporal variability of suspended sediments in rivers and ecological implications of reservoir flushing operations. River Res. Appl. 35 (7), 918–931. http://dx.doi.org/10.1002/rra.3492.

Tritthart, M., Schober, B., Habersack, H., 2011. Non-uniformity and layering in sediment transport modelling 1: Flume simulations. J. Hydraul. Res. 49 (3), 325–334. http://dx.doi.org/10.1080/00221686.2011.583528.

Vanzo, D., Adami, L., Siviglia, A., Zolezzi, G., Vetsch, D.F., 2017. The role of numerical diffusion in river alternate bar simulations. In: 10th Symposium on River, Coastal and Estuarine Morphodynamics (RCEM 2017): Book of Abstracts. RCEM2017 Organizing Commitee, 253–253.

Vanzo, D., Peter, S., Vonwiller, L., Bürgler, M., Weberndorfer, M., Siviglia, A., Conde, D., Vetsch, D.F., 2021. BASEMENT v3: A modular freeware for river process modelling over multiple computational backends. Environ. Model. Softw. 143, 105102. http://dx.doi.org/10.1016/j.envsoft.2021.105102.

Vargas-Luna, A., Crosato, A., Byishimo, P., Uijttewaal, W.S.J., 2018. Impact of flow variability and sediment characteristics on channel width evolution in laboratory streams. J. Hydraul. Res. 1–11. http://dx.doi.org/10.1080/00221686.2018.1434836.

Vetsch, D.F., Frei, S., Halso, M.C., Schierjott, J.C., Bürgler, M., Vanzo, D., 2023. Basement V4—A multipurpose modelling environment for simulation of flood hazards and river morphodynamics across scales. In: SimHydro. Springer, pp. 125–138.

Volp, N., van Prooijen, B., Pietrzak, J., Stelling, G., 2016. A subgrid based approach for morphodynamic modelling. Adv. Water Resour. 93, 105–117. http://dx.doi.org/10.1016/j.advwatres.2015.07.013.

van der Wegen, M., Jaffe, B.E., 2014. Processes governing decadal-scale depositional narrowing of the major tidal channel in San Pablo Bay, California, USA. J. Geophys. Res.: Earth Surface 119 (5), 1136–1154. http://dx.doi.org/10.1002/2013JF002824.

Wilcock, P.R., Crowe, J.C., 2003. Surface-based transport model for mixed-size sediment. J. Hydraul. Eng. 129 (2), 120–128. http://dx.doi.org/10.1061/(ASCE)0733-9429(2003)129:2(120).

Williams, R.D., Brasington, J., Hicks, D.M., 2016. Numerical modelling of braided river morphodynamics: Review and future challenges. Geography Compass 10 (3), 102–127. http://dx.doi.org/10.1111/gec3.12260.

Zimmerman, C., Kennedy, J.F., 1978. Transverse bed slopes in curved alluvial streams. J. Hydraulics Div. ASCE 104 (1), 33–48. http://dx.doi.org/10.1061/JYCEAJ.0004922.